CrystEngComm

PAPER

View Article Online
View Journal | View Issue

Cite this: *CrystEngComm*, 2023, **25**, 3609

New hybrid: [H-β-(4-pyridyl)-Ala-OH] tetrafluoroborate – crystal structure and strong piezoelectricity†

Maciej Wojtaś, *[a] Tamara J. Bednarchuk[b] and Igor Bdikin[c]

Received 30th March 2023,
Accepted 16th May 2023

DOI: 10.1039/d3ce00308f

rsc.li/crystengcomm

A new amino acid based crystal [H-β-(4-pyridyl)-Ala-OH][BF_4] was synthesized. The structure was determined using single-crystal diffraction. The title salt crystallizes in the polar, piezoelectric $P2_1$ space group. It was demonstrated by means of piezoelectric force microscopy that the piezoresponse of the [H-β-(4-pyridyl)-Ala-OH][BF_4] crystal is higher than that of lithium niobate, $LiNbO_3$. The crystal structure, specifically the hydrogen bond network, and the physical properties of the alanine derivative were correlated. The thermal behavior of the title crystal was studied by means of thermogravimetric analysis (TGA). The high piezoresponse of [H-β-(4-pyridyl)-Ala-OH][BF_4] and other alanine salts was discussed.

1 Introduction

A common feature of non-centrosymmetric materials is piezoelectricity. Such compounds, due to the direct piezoelectric effect, when subjected to mechanical stress generate an electric charge proportional to that stress, and due to the converse piezoelectric effect generate mechanical stress when an electric field is applied. These effects where discovered by the Curie brothers in the late 19th century,[1] and one of the first applications of piezoelectric materials was in sonar which was developed during World War I by the Paul Langevin group.[2] Nowadays piezoelectrics are used in many applications, such as actuators, sensors, acoustic transducers and piezomotors.[3]

Piezoelectrics which possess a polar axis may exhibit so-called ferroelectric hysteresis loops (P–E loops)[4] *i.e.* the polarization direction can be altered by an external electric field. These materials are called ferroelectrics. Their piezoelectric constants are significantly higher than those found in nature such as some bio-organic materials (*e.g.*, lamellar-bone, collagen).[5,6] Due to this property, ferroelectrics are applied in the areas of microelectronics and micromechanical systems, which include field effect transistors and nonvolatile memories.[7,8] Recently, organic ferroelectrics have been gaining ground over previously used inorganic ones. This is due the fact that, compared to inorganic piezoelectrics, organic compounds have two main advantages: lower cost and the ability to use chemical methods to alter the structure. Therefore, significant progress in the search for new organic ferroelectrics has been observed in recent years.[9,10] Such materials include many organic biomaterials due to their natural asymmetry and the presence of polarized bonds. These features are common for amino acids, peptides and proteins. It was suggested by Gazit[11] and shown by Görbitz[12–14] that an alanine derivative, L-phenylalanyl-L-phenylalanine, which easily self-assembles in tube-like structures, belongs to the group of most promising materials for nanoelectronic applications. Not long later, Kholkin *et al.*[15] showed that peptide nanotubes exhibit a strong piezoelectric effect with the orientation of polarization along the axis of the tube. The magnitude of this effect was comparable with lithium niobate, $LiNbO_3$ (LNO).

Recently, our research has been extended to hybrid, organic–inorganic materials. They comprise selected, voluminous amino acids presented in Fig. 1 and simple, small inorganic acids, such as $HClO_4$ and HBF_4.[16,17]

[a] *Faculty of Chemistry, University of Wrocław, 14 Joliot-Curie, 50-383 Wrocław, Poland. E-mail: maciej.wojtas@uwr.edu.pl*
[b] *Institute of Low Temperature and Structure Research, Polish Academy of Sciences, Okólna 2, 50-422, Wrocław, Poland*
[c] *TEMA, Mechanical Engineering Department, University of Aveiro, 3810-193 Aveiro, Portugal*

† Electronic supplementary information (ESI) available. CCDC 2247731. For ESI and crystallographic data in CIF or other electronic format see DOI: https://doi.org/10.1039/d3ce00308f

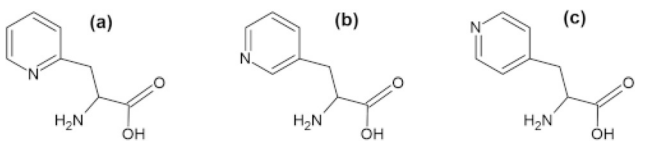

Fig. 1 The plain structural formula of (a) [H-β-(2-pyridyl)-Ala-OH]; (b) [H-β-(3-pyridyl)-Ala-OH] and (c) [H-β-(4-pyridyl)-Ala-OH].

It has been demonstrated that the tetrafluoroborate derivative of 2-pyridyl alanine exhibits high piezoelectricity, higher than those of lithium niobate. Moreover, the title crystal is characterized by the highest piezoelectric modules comparing to other compounds of this group. This paper presents complementary studies including X-ray diffraction, thermogravimetry, infrared and Raman spectroscopy, and piezoresponse force microscopy (PFM) of the title alanine derivative, [H-β-(4-pyridyl)-Ala-OH][BF_4].

2 Experimental

The title crystal was prepared by the reaction of [H-β-(4-pyridyl)-Ala-OH] ((*S*)-2-amino-3-(pyridin-4-yl)-propionic acid, Bachem) with tetrafluoroboric acid (50%, POCh) in water solution. The solutions were then dried under ambient conditions and yielded small, colorless, needle-shaped crystals. The elemental analysis results agreed well with the proposed formula: [H-β-(4-pyridyl)-Ala-OH][BF_4] (hereafter abbreviated as [4PyAla][BF_4]): N: 10.92%; C: 37.32%, H: 4.21% (theoretical N: 11.02%; C: 37.83%, H: 4.33%). The samples for the AFM(PFM) measurements were prepared by drying a drop of the water solution of [4PyAla][BF_4] on a platinum coated silicon substrate.

Crystallographic data for the compound [4PyAla][BF_4] were collected on a Xcalibur four-circle diffractometer equipped with a two dimensional CCD detector and MoKα radiation (λ = 0.71073 Å) at 100 K. The instrument was equipped with an Oxford Cryosystems 800 series cryocooler. Data collection and reduction including empirical absorption corrections was performed using the CrysAlisPro program.[18] The crystal structure was solved by direct methods and refined on F^2 by a full-matrix least-squares method using SHELXT and SHELXL-2014/7 crystallographic software package[19] available with the Olex2-1.5 interface.[20] Anisotropic displacement parameters were applied for all non-hydrogen atoms. The positions of the H atoms of the cationic moieties were initially located in the difference Fourier maps, and for the final refinement, the H atoms were incorporated in the geometric positions and treated as riding atoms (HFIX command). The thermal parameters of the hydrogen atoms were set to be equal to 1.2 times the thermal parameters of the corresponding parent atoms. The Diamond 3.2 program[21] was used to produce the molecular graphics. The geometry of stacking π···π and B–F···π intermolecular interactions were analyzed using the PLATON program.[22] Crystallographic data and details of data collection and refinement are given in Table 1; selected distances and angles are listed in Table S1 in the ESI.†

Thermogravimetric analysis (TGA) and differential thermal analysis (DTA) for the investigated compound were performed in the 298–900 K temperature range using a Setaram SETSYS 16/18 instrument. The sample weight was 9.340 mg. The heating speed rate was 5 deg min^{-1}. The scan of the ground sample placed in the open crucible was performed in flowing nitrogen.

Table 1 Crystal data, experimental details and structure refinement results for [4PyAla][BF_4]

Crystal data	
Chemical formula	$C_8H_{11}N_2O_2{\cdot}BF_4$
M_r	254
Crystal system, space group	Monoclinic, $P2_1$ (no. 4)
Temperature (K)	100
a, b, c (Å)	5.355(3), 8.831(3), 11.415(4)
β (°)	90.79(3)
V (Å^3)	539.8(4)
Z	2
Absorption coefficient, μ (mm^{-1})	0.15
Crystal size (mm)	013 × 0.05 × 0.04
Data collection	
Diffractometer	Xcalibur, Atlas
Absorption correction	Multi-scan
T_{min}, T_{max}	0.974, 1.000
No. of measured, independent, and observed [$I > 2\sigma(I)$] reflections	10 961, 2063, 1909
R_{int}	0.047
$(\sin\Theta/\lambda)_{max}$ (Å^{-1})	0.61
Refinement	
$R[F^2 > 2\sigma(F^2)]$, w$R(F^2)$, S	0.045, 0.115, 1.05
No. of reflections	2063
No. of parameters	155
No. of restraints	1
H atoms treatment	H-atom parameters constrained
$\Delta\rho_{max}$, $\Delta\rho_{min}$ (e Å^{-3})	0.31, −0.24
Absolute structure parameter	−0.2(6)

The room temperature FT-IR spectra (Fluorolube and Nujol mulls, polyethylene windows) were measured using a BRUKER 66 spectrometer with the resolution of 2 cm^{-1}.

The Raman spectrum was collected using a Thermo Scientific Nicolet iS50 Raman module mounted in the sample compartment of a Thermo Scientific Nicolet iS50 FTIR spectrometer. An indium–gallium arsenide (InGaAs) detector and CaF_2 beamsplitter were used to carry out the measurements. The sample was illuminated by a 1.064 μm O_4 laser with a power of 250 mW. The interferogram was averaged over 256 scans, Happ–Genzel apodized, and Fourier transformed using a zero-filling factor of 2 to yield spectra in the 200–3700 cm^{-1} range with a resolution of 2 cm^{-1}.

Atomic force microscopy (AFM) measurements were carried out using a Veeco AFM Multimode Nanoscope (IV) MMAFM-2, Veeco microscopy. Local piezoelectric properties of the sample were visualized simultaneously by using AFM in contact mode and PFM methods. The PFM technique is based on the converse piezoelectric effect, which is a linear coupling between the electrical and mechanical properties of a material. To detect the polarization orientation, the AFM tip is used as a top electrode, which is moved over the sample surface. For PFM imaging, doped (n^+) Si cantilevers with resistivity of 0.01–0.02 cm and tip apex radius of less than 10 nm with a spring constant of 7.4 N m^{-1} were used

(Nanosensors). An AC voltage of 5 V at a frequency of 35 kHz was applied. The measurement frequency was chosen far away from the resonant frequencies of the cantilever sample-holder system to avoid the ambiguity of experimental data.

3 Results and discussion

3.1 Crystal structure

The compound [4PyAla][BF_4] crystallizes in the monoclinic polar $P2_1$ space group with $Z = 2$. The asymmetric part of the unit cell contains one protonated 3-(4-pyridyl)alanine cation and one tetrafluoroborate anion, both laying in crystallographic general positions (Fig. 2). In the BF_4^- anion all four F atoms are characterized by elongated displacement ellipsoids. The geometric features of tetrafluoroborate anion indicate a distorted tetrahedral configuration: the B–F bond lengths range from 1.372(6) to 1.394(6) Å, whereas the corresponding F–B–F angles vary from 106.8(4) to 113.0(5)° (Table S1 in the ESI†). In a previously published work, we presented the crystal structure of [H-β-(2-pyridyl)-Ala-OH][BF_4], in which the distortion of the tetrahedral geometry was much larger due to the disorder.[16] The organic cation comprises a protonated amine group and a negatively charged carboxylate group, while protonation on the pyridine group carries a positive charge of the molecule. The C2–N1 distance is 1.491(4) Å, which is characteristic for a single bond, indicating protonation of the amine nitrogen atom. The almost equal C–O bond distances (1.248(4) and 1.255(4) Å) are consistent with the deprotonated carboxyl group. Confirmation of the proton transfer to the pyridine N atom is revealed by the widening of the C12–N11–C16 bond angle of the aromatic ring to 120.8(4)°. The conformation of the 3-(4-pyridyl)alanine cation is somewhat similar to one of the two crystallographically independent organic molecules (B) in the structure of the aforementioned tetrafluoroborate derivative of 2-pyridyl alanine.[16] In both these cations, the carboxylate groups are deviated and oriented away from the aromatic ring, so there is no intramolecular N/C–H···O hydrogen bonding. On the other hand, the conformation of the cations in the described compound and the perchlorate derivative of 4-pyridyl alanine,[17] which also crystallizes in the polar space group $P2_1$, differ more significantly. In the latter compound, the side chain is twisted and bent, compared to the more straightened chain in [4PyAla][BF_4]. As a result, the carboxylate group is oriented toward the pyridinium ring and forms an intramolecular C–H···O hydrogen bond, while the NH_3^+ group and the α-carbon are directed to the perchlorate ion, forming two weak N–H···O and C–H···O hydrogen bonds. In contrast to the former material, the conformation of the cation in the title compound, as shown in Fig. 2, promotes the formation of a moderately strong N1–H1A···F1 hydrogen bond. Among all intermolecular hydrogen bonds observed in the crystal structure of [4PyAla][BF_4] (Fig. 3a, Table 2), two general types of interactions can be distinguished: connections between adjacent cations and between counter-ions. Neighbouring cations are linked into infinite chains along the *a* axis by N1–H1C···O1 bonds, while the N1–H1C···O2 hydrogen bonds form a second chain parallel to the *b* direction (Fig. 3a). These intermolecular contacts between symmetry-related molecules through the ammonium group of the 3-(4-pyridyl)alanine cation and carboxylate groups are the strongest in the crystal structure of [4PyAla][BF_4]. The hydrogen-bonded arrangement generated by the first type of interactions leads to the formation of two-dimensional layers in the *ab* plane. Weak non-covalent C–H···O interactions involving α and β hydrogen atoms further stabilize the aforementioned layer. Fig. 3c shows the second type of interactions, in which an inorganic anion acts as an acceptor for three moderately strong N–H···F and three

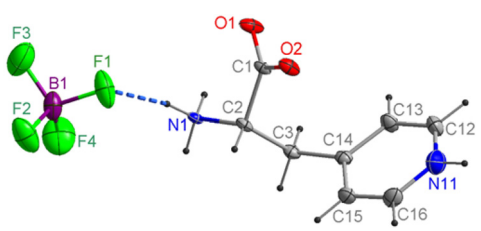

Fig. 2 The molecular structure of [4PyAla][BF_4] showing the atom-numbering scheme and N–H···F interaction (light blue dashed line). Displacement ellipsoids for non-H atoms are drawn at the 50% probability level.

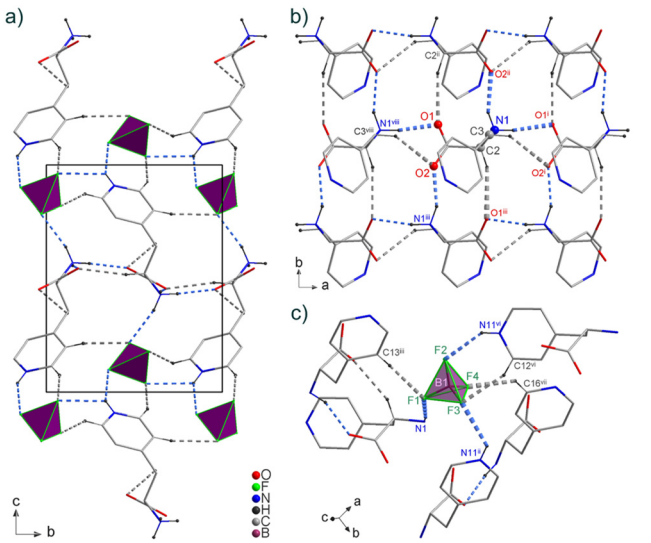

Fig. 3 (a) Packing view of [4PyAla][BF4], projected along the *a* axis. Part of the crystal structure represents: (b) a fragment of the hydrogen-bonding cationic layer viewed parallel to the *ab* plane; (c) an interaction of the BF_4^- anion with adjacent counterions. The blue and grey dashed lines indicate N–H···O/F and C–H···O/F hydrogen bonds. (b and c) Bold hydrogen bonds refer to symmetrically independent cations or anions. Hydrogen atoms not involved in bonding are omitted for clarity. Symmetry codes: (i) $x + 1, y, z$; (ii) $-x + 1, y + 1/2, -z + 1$; (iii) $-x + 1, y - 1/2, -z + 1$; (vi) $x + 1, y, z - 1$; (vii) $-x + 2, y + 1/2, -z + 1$; (viii) $x - 1, y, z$.

Table 2 Selected hydrogen-bond parameters for [4PyAla][BF_4]

D–H···A	D–H (Å)	H···A (Å)	D···A (Å)	D–H···A (°)
HBs between cations				
N1–H1B···O1^{i}	0.91	1.83	2.733(4)	170
N1–H1C···O2^{ii}	0.91	1.89	2.741(4)	156
C2–H2···O1^{iii}	1	2.41	3.362(5)	159
C3–H3A···O2^{i}	0.99	2.58	3.318(4)	132
HBs between counter-ions				
N1–H1A···F1	0.91	2.03	2.922(4)	165
N11–H11···F2^{iv}	0.88	2.24	2.994(5)	144
N11–H11···F3^{iii}	0.88	2.4	2.995(6)	125
C16–H16···F4^{v}	0.95	2.26	2.958(5)	130
C13–H13···F1^{ii}	0.95	2.33	3.265(5)	168
C12–H12···F3^{iv}	0.95	2.36	3.227(6)	152

Symmetry codes: (i) $x + 1, y, z$; (ii) $-x + 1, y + 1/2, -z + 1$; (iii) $-x + 1, y - 1/2, -z +$ (iv) $x - 1, y, z + 1$; (v) $-x + 2, y - 1/2, -z + 1$.

weak C–H···F hydrogen bonds. All F atoms make these contacts with the pyridinium ring, and only the F1 atom accepts one of the two hydrogen bonds from the protonated NH_3^+ group. These hydrogen bonding cause anions to act as linkers to neighboring cations along the *c* axis direction, forming a 3D framework structure (Fig. 3a). The organic cations form parallel columns along the *a* axis (Fig. 3a and b), with the centroid–centroid distances between the pyridine rings of 5.355(4) Å and an offset of 4.148 Å [symmetry code: $1 + x, y, z; -1 + x, y, z$;]. Therefore, it can be assumed that the aromatic π–π stacking interactions are absent from the structure of the title compound. As shown in Fig. S1 and Table S2 (ESI†), the F3 atom of the BF_4^- anion interacts with the centroid of the neighbouring ring (3.030(4) Å, symmetry code: $x, -1 + y, z$). This anion···π interaction interconnects the adjacent molecules along the *c* axis and promotes crystal cohesion.[23,24]

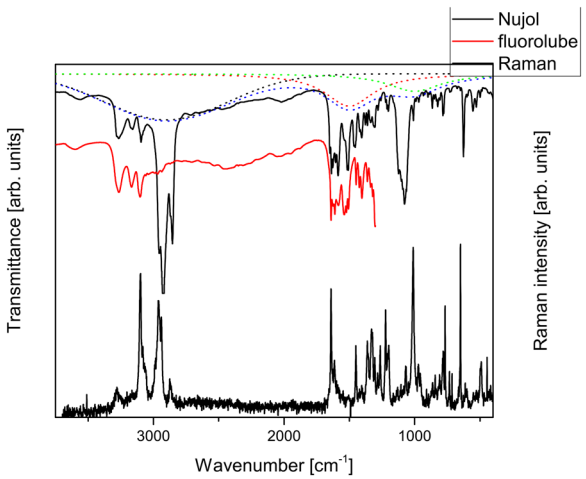

Fig. 4 Infrared (Nujol and Fluorolube oil) and Raman spectra of [4PyAla][BF_4]. The dashed lines show Hadži's trio and its sum for the compound.

3.2 IR and Raman measurements

The experimental IR and Raman spectra of the title compound are presented in Fig. 4. IR spectra were recorded in Fluorolube and Nujol oil at ambient conditions. A characteristic of the IR spectrum in Nujol is broad and intense absorption. This result may be described based on Hadži's trio[25] theory. Therefore it was possible to fit to the IR spectrum three components. The wavenumbers of their maxima are 2906, 1480 and 986 cm^{-1}. The model of the Hadži's trio[25] indicates that the lattice phonons interfere the coupling of the hydrogen bridge vibrations.[26] It causes the anharmonic stretching vibrations of the proton in the hydrogen bond which may be explained on the basis of Samorjai's approach.[27] Thus, the proton dynamic is characterized by an asymmetric double minimum potential and may be expressed by:

$$V(r, R) = a_2(R)r^2 + a_3(R)r^3 + a_4(R)r^4,$$

where r is the coordinate of the proton movement, R stands for the coordinate of the hydrogen bridge vibration and a_2, a_3 and a_4 are R dependent parameters. The frequencies and assignments of the bands observed in the Raman and IR spectra are presented in Table 3. The assignments are proposed based on ref. 28–30.

3.3 Thermal behaviour

Fig. 5 presents the TGA measurements of the [4PyAla][BF_4] sample.

The title crystal remains thermally stable up to *ca.* 400 K which is lower than that of the other 2-pyridyl and 3-pyridyl alanine derivatives studied by us. At this temperature one can observe a little weight loss (≈4%) accompanied by 2 endothermic peaks at 420 K and 447 K. Subsequent weight loss of ≈23% is linked with an endothermic effect manifested as a peak with maximum at 478 K. The consecutive decomposition finishes at around 700 K, where the residue is *ca.* 15% of the initial mass of the sample. This process is accompanied by two merged peaks with maxima at 550 K and 610 K. After Y. C. Lien and W. W. Nawar[31] as well as A. Schaberg *et al.*[32] one may assign the first change of mass to the loss of ammonia and the second one to the loss of carbon dioxide/carbon monoxide.

3.4 PFM measurements

Fig. 6a and b presents the AFM images of the size 50 × 50 μ^2 which were acquired in contact mode. The topography, out-of-plane (OOP) and in-plane (IP) piezoresponse signals were recorded simultaneously and on the figure the topography and topography with the OOP signal in 3d-view are presented.

It is noteworthy that the majority of the microcrystals have an elongated cuboidal shape which is common for either tetrafluoroborate or perchlorate phenylalanine salts.[16,17] Another important feature of the sample is the negative offset

Table 3 Vibrational frequencies (wavenumbers, cm^{-1}) of [4PyAla][BF4] recorded in ambient conditions

Raman	IR	Assignments
	3563w, 3563w[f]	
3278w	3280s, 3284s[f]	Asym. NH_2 stretch.
	3166m,[f] 3162w	Sym. NH_2 stretch.
3098vs, 3080m, 3066sh	3102m,[f] 3097w	Asym. NH_3 stretch and C–H aromatic
2982sh, 2961s, 2939s	2955vs,[n] 2931vw[f]	
	2932m, 2931s[f]	
	2924vs,[n] 2867sh	
2875m	2864vs[n]	
	2710vw,[f] 2709vw	
	2567vw, 2537vw[f]	NH stretch. in NH_3
	2459vw[f]	
	2347vw[f]	Stretch. CNH bend
	2252vw[f]	
	2066vw[f]	
	1952vw[f]	
1638vs	1650m, 1641s,[f] 1637s	NH_2 bend.
	1624s,[f] 1623s	
1612m	1610s,[f] 1605m, 1586s	(C═N) conjugated
	1582m[f]	
1550w	1540sh, 1540s[f]	NH_3 puckering
1502w	1522 m,[f] 1516s, 1508s	C═C and
	1505m[f]	C═N conjugated
1449s, 1443sh, 1428vw	1465m,[n] 1463m,[n] 1449s[f]	CH_2 bend
1422w, 1404w, 1398w	1425s,[f] 1420m, 1406m,	
1392vw	1404s[f]	
1380w, 1374sh	1376w, 1363m,[f] 1360w	CH_3 bend
	1346sh,[f] 1343sh, 1337w	
	1337w,[f] 1322w[f]	
1362s	1360w	NH_3 puckering
1351sh, 1345m, 1330s	1346sh,[f] 1343sh,1337w	
	1337w[f]	
1321s, 1303m	1322w,[f] 1306w	CN stretch
1291w, 1282m, 1274w	1280w, 1260w	
1263s, 1241w		
1223vs, 1205m, 1196s	1222w, 1211w, 1201w	
1179vw, 1173vw		
1164w, 1152w, 1137w, 1129w	1162sh	
1110w, 1102w, 1093vw	1123vs, 1102s, 1092s	NH bend
1082vw, 1072sh, 1068m	1078vs, 1064s	
1065m, 1057w, 1048w		
1043vw, 1040vw, 1036vw		
1028sh, 1011vs	1009w	H_3–N_1–C_2–C_3 bend
987w, 971m, 957w, 950sh	991vw, 969vw	Asym NC_2 stretch
942w, 932vw, 928vw	933vw, 924vw	
918vw, 907w, 899vw	900vw, 886vw, 865w	Sym NC_2 stretch
894w, 883vw, 873w	847vw, 832vw, 823w	
861w, 852w, 843w		
836w, 832vw, 820w		
808w, 801w		
793sh, 786m, 780m	806vw, 784w, 777w	NH_2 rocking
777m, 767s, 749vw		
740vw, 733m, 723w	731vw, 720vw	HNC bend
719vw, 713m, 703w		
694vw, 688vw, 677vw		
677vw, 664w, 649vs	674vw, 650vw	OCOH + NH_2 bend
642w, 627w	626s	
612w, 606vw, 600w	598vw, 593vw	
584vw, 578vw		
550w, 546vw, 541vw	553w, 528w	OH bend
532w, 526w, 520w, 514vw		
509w, 496m, 490m	499w, 484vw	
478vw, 474vw, 467w, 464w		
,458vw, 452vw, 450vw		
445m, 439w, 435w, 431w		
426w, 418w, 415w, 410vw		
408vw, 403vw, 399w		
394vw, 383w		

Table 3 *(continued)*

Raman	IR	Assignments
376vw, 371w, 366w, 361w		
357w, 348w, 343w, 339vw		
334vw, 328vw, 326vw		
320vw, 314sh		
307m, 303m, 300sh		
292w, 286vw, 282w		
275vw, 271vw		
267w, 264vw, 261vw, 258vw		
250vw, 244vw, 240vw, 235vw		
233vw, 228vw, 225vw		
216s, 211s, 205s		

^{n} = bands of Nujol oil; ^{f} = bands observed in Fluorolube oil.vs, very strong; s, strong; m, medium; w, weak; vw, very weak; sh, shoulder.

of the piezoresponse, which may indicate that the polarization of the adjacent crystals affect each other, which works in favor of the same polarization direction. Nevertheless the piezoresponse is characterized by a significant contrast in the magnitude of recorded signal which is not directly related to the topography of the sample.

Direct proof of the sample's piezoelectricity is provided by measurements of piezoresponse *vs.* an AC electric field (driving voltage). However, due to the inhomogeneous distribution of the electric field,[33] we are only able to qualitatively estimate the effective piezoresponse. In order to quantify the values of piezoelectric modulus of [4PyAla][BF_4], we compared the piezoresponse with that of lithium niobate, $LiNbO_3$ – commercially available (NT-MDT), periodically poled lithium niobate, and cut normal to the polar axis. In this way, it was possible to determine the magnitude of the piezoeffect in the sample, avoiding rigorous calculations.[34] Moreover, in the case of [4PyAla][BF_4] sample there is a distribution of the piezo signal (see Fig. 6), which indicates the distribution of different grain orientations. It has been shown by Bdikin *et al.*[35] that if we are dealing with a distributed orientation of grains, it is possible estimate piezoelectric coefficients. Although the exact orientation of microcrystals was unknown, we proposed a random distribution and we analysed the sample with maximum OPP and IP signals and therefore we were able to estimate effective piezoelectric modules. The resulting graphs of the piezoelectric response *vs.* electric field applied are presented in Fig. 7a and b.

Based on the following matrix[36] of the piezoelectric modulus of the point group 2 with standard axes orientation,

$$\begin{bmatrix} \cdot & \cdot & \cdot & d_{14} & \cdot & d_{16} \\ d_{21} & d_{22} & d_{23} & \cdot & d_{25} & \cdot \\ \cdot & \cdot & \cdot & d_{34} & \cdot & d_{36} \end{bmatrix},$$

where a light dot stands for a modulus that is zero, one may conclude that the longitudinal deformation ($d_{33,\mathrm{eff}}$) of the sample is mainly due to the application of the electric field

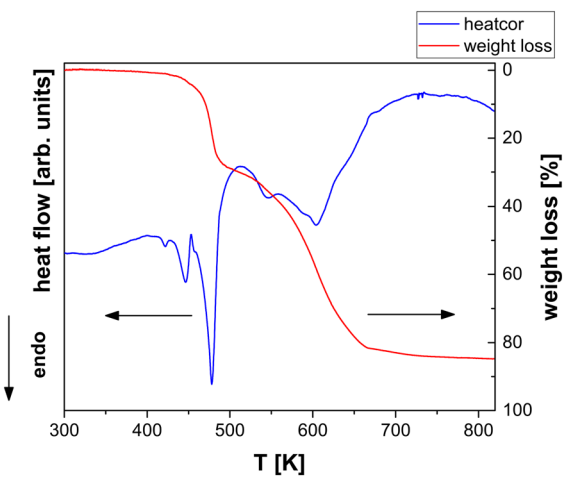

Fig. 5 TGA scans of [4PyAla][BF_4]. The scans were performed in flowing nitrogen with a ramp rate of 5 deg min^{-1}, sample mass 9.340 mg.

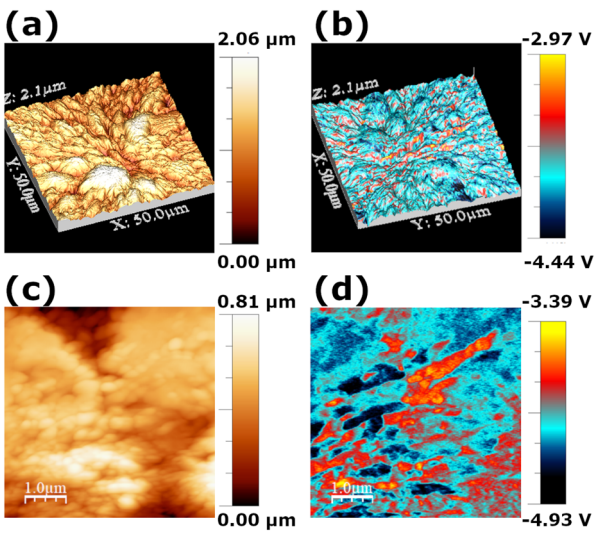

Fig. 6 AFM images of [4PyAla][BF_4] sample. (a) Topography (3D view); (b) topography with OOP piezoresponse (3D view); (c) topography (2D view); (d) topography with piezoresponse (2D view).

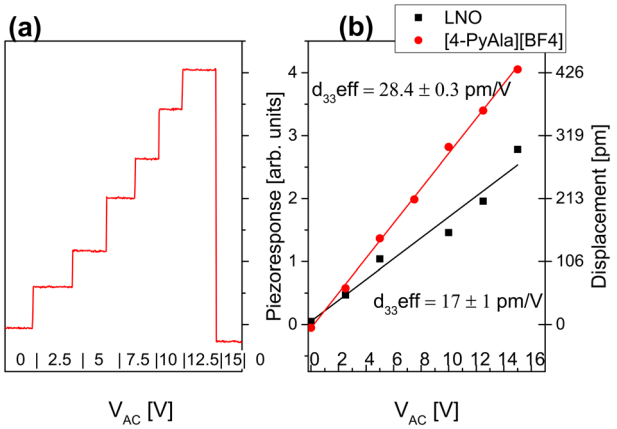

Fig. 7 (a) OOP piezoresponse of [4PyAla][BF_4] *vs.* driving voltage. (b) Driving voltage dependence of OOP piezoresponse of LNO and [4PyAla][BF_4].

along the *b*-direction. Besides that, the shear deformation ($d_{15,\mathrm{eff}}$) may be observed independent of the direction of the electric field applied. However, since the orientation of the microcrystals is nonuniform, the effective piezoresponse of the sample is affected by both longitudinal and shear components of the piezoelectric modulus. The driving voltage dependence of IP piezoresponse of LNO and [4PyAla][BF_4] is shown in Fig. S3 in the ESI.†

3.5 Discussion

The title crystal, [4PyAla][BF_4], is another representative of the amino acid based hybrid crystals. It crystallizes in the polar $P2_1$ space group. The most important feature of [4PyAla][BF_4] is its piezoelectricity, whose response under the influence of the applied electric field is significantly higher to that of LNO. The piezoelectric modulus of the remaining amino acid based hybrids are listed below.

Crystal		Space group	Piezoelectric module	
Cation	Anion		Longitudinal	Shear
[H-β-(2-Pyridyl)-Ala-OH]	ClO_4^-	$P2_12_12_1$	0	3
[H-β-(3-Pyridyl)-Ala-OH]		$P2_1$	18	39
[H-β-(4-Pyridyl)-Ala-OH]		$P2_1$	6	20
[H-β-(2-Pyridyl)-Ala-OH]	BF_4^-	$P1$	19	41
[H-β-(4-Pyridyl)-Ala-OH]		$P2_1$	28	79

The high values of the piezoelectric modulus are common for all the investigated hybrid crystals. Since they crystallize in quite a low symmetry, the piezoresponse depends on several piezoelectric coefficients. The only exception is $HClO_4$, $X = 2$, which exhibits the lowest piezoresponse and is characterized by the highest symmetry in the group of alanine based hybrids. Only in this case the piezoresponse is related to only one piezoelectric coefficient – the longitudinal d_{33} which is 0 and the shear, either d_{25} or d_{36} (see discussion in ref. 16). In general, the lower the symmetry of the crystal the higher the piezoresponse. This observation must be due to the number of piezoelectric coefficients contributing to the effective piezoresponse, both $d_{33,\mathrm{eff}}$ (longitudinal) and $d_{15,\mathrm{eff}}$ (shear). Also, from a crystallochemical point of view, the influence of the anion subnetwork on piezoelectric properties seems to be interesting. The perchlorate anion is slightly larger than the tetrafluoroborate anion, so it takes up more space. Consequently, it creates more hydrogen bonds with neighboring organic cations. However, there are many of factors that can affect the molecular geometry of the cation and it is very difficult to estimate the special role of the anions in the conformational change of the cations.

Another factor which affects the piezoelectric properties of the studied crystals is the crystallochemistry. Hydrogen bonding parameters seem to be the most important. In the group of perchlorate salts the piezoelectric coefficient significantly depends on the strength of the hydrogen bonds – the stronger the H-bonds, the lower the piezoelectric coefficient. The criterion for assessing the strength of the bonds was their geometry – donor–acceptor distances and donor–H–acceptor angles.[37] The case of tetrafluoroborate derivatives confirms the conclusion drawn for perchlorate compounds. In the investigated crystal herein, 2 hydrogen bonds between the cations (N–H⋯O) and 2 between the counter-ions (N–H⋯F) can be distinguished. The donor–acceptor distances in N–H⋯O interactions are 2.733(4) Å and 2.741(4) Å and the donor–proton⋯acceptor angles are 170° and 156°. The N–H⋯F bonds are characterized by the donor–acceptor distances of the order of 2.9 Å and donor–proton⋯acceptor angles being 165° and 144° (see Table 2). In the case of [2PyAla][BF_4], one can distinguish 3 H-bonds between the cations and 2 H-bonds between the counterions at least. The geometrical parameters (donor–acceptor distance/donor–proton–acceptor angle) are *ca.* 2.6 Å/159°, 2.8 Å/172°, 2.7 Å/168° and 2.8 Å/163°, 2.7 Å/143° (see ref. 16). Moreover, in [2PyAla][BF_4], the fluorine atoms in tetrafluoroborate anions take part in 9 important H-bonds whereas in the title crystal they participate just in 3. A similar observation can be made for cation interactions: 5 to 2 in favor for [2PyAla][BF_4]. The consequence of this state of affairs is a higher value of the piezoelectric $d_{33,\mathrm{eff}}$ coefficient of [4PyAla][BF_4] compared to [2PyAla][BF_4].

It is worth noting that the amino acid derivatives exhibit nonlinear optical (NLO) properties due to the presence of the chiral carbon atom.[38–40] Beside this the hybrid salts studied by us are characterized by high values of piezoelectric modulus and are mostly polar. The synthesis of salts with the incorporation into their structure other heterocyclic compounds can result to the emergence of ferroelectricity in them.[41] The number of possible modifications to obtain materials with the desired properties seems to be unlimited.

It is also worth emphasizing that amino acid based materials are much safer for environment than lead

containing compounds like $Pb[ZrTi]O_3$. In addition, these traditional piezoelectric materials are intrinsically incompatible with biological tissues and will be eventually prohibited for its use.[42] It is therefore advisable to search for compounds which are suitable for biomedical applications and possessing interesting physical properties (piezo-, pyro-, ferroelectricity). The former may be realized by the incorporation of biologically active molecules such as amino acids. From this point of view, studies on amino acid based hybrid crystals are important and may facilitate the prediction of the structures which satisfy these demands. Moreover, the investigation of single crystals eases finding the possible correlation between the functional properties and structure. For this reason, amino acid based hybrids may be suitable for application.

4 Conclusions

To conclude, we have unveiled a structure of another member of the family of hybrid crystals made of pyridyl alanine derivatives and small inorganic acids. The crystal has been studied by a wide range of analytical techniques, such as: X-ray diffraction, thermogravimetry, IR and Raman spectroscopy, and PFM. The most striking feature of [4PyAla][BF_4] is its piezoelectric response – almost 2 times greater than that of lithium niobate (LNO). Moreover, it was found that there is a strong correlation between piezoelectric properties and hydrogen bonding structure. The hydrogen bonds play a dominant role in stabilizing and stiffening the structure, which affects the piezoelectric response of [4PyAla][BF_4]. Furthermore, weak electrostatic interaction *via* hydrogen bonds can change deformation of piezoelectric material which occurs as a result of an applied electric field. This electromechanical response plays a decisive role in a number of potential applications. Due to the possibility of incorporating different organic ions, we strongly believe that we are approaching the possibility of modifying the physical properties of amino acid hybrids.

Conflicts of interest

There are no conflicts to declare.

Acknowledgements

M. W. would like to thank Prof. Roman Szostak for carrying out the measurements of the Raman spectroscopy. I. B. acknowledges the Portuguese Science Foundation (FCT) for the financial support of project CARBONCT (2022.03596.PTDC).

Notes and references

1 J. Curie and P. Curie, *Bull. Soc. Fr. Mineral.*, 1880, **3**, 90.
2 P. Biquard, *Ultrasonics*, 1972, **10**, 213–214.
3 A. Safari and K. Akdogan, *Piezoelectric and Acoustic Materials for Transducers Applications*, Springer, New York, 2008.
4 M. Wojtaś and M. J. Reece, *J. Appl. Phys.*, 2012, **111**, 024108.
5 E. Fukada and I. Yasuda, *J. Phys. Soc. Jpn.*, 1957, **12**, 1158–1162.
6 E. Fukada and I. Yasuda, *Jpn. J. Appl. Phys.*, 1964, **3**, 502B.
7 A. J. Lovinger, *Science*, 1983, **220**, 1115.
8 S. Das and J. Appenzeller, *Nano Lett.*, 2011, **11**, 4003.
9 R. C. G. Naber, C. Tanase, P. W. M. Blom, G. H. Gelinck, A. W. Marsman, F. J. Touwslager, S. Setayesh and D. M. Leeuw, *Nat. Mater.*, 2005, **4**, 243.
10 A. Piecha, A. Gągor, R. Jakubas and P. Szklarz, *CrystEngComm*, 2013, **15**, 940.
11 E. Gazit, *Chem. Soc. Rev.*, 2007, **36**, 1263.
12 C. H. Görbitz, *Chem. – Eur. J.*, 2001, **7**, 5153.
13 C. H. Görbitz, *New J. Chem.*, 2003, **27**, 1789.
14 C. H. Görbitz, *Chem. Commun.*, 2006, 2332.
15 A. Kholkin, N. Amdursky, I. Bdikin, E. Gazit and G. Rosenman, *ACS Nano*, 2010, **4**, 610.
16 M. Wojtaś, A. Gągor and A. L. Kholkin, *J. Mater. Chem. C*, 2016, **4**, 7622–7631.
17 M. Wojtaś, V. Kinzhybalo, I. Bdikin and A. Kholkin, *Cryst. Growth Des.*, 2019, **19**, 2583–2593.
18 Rigaku Oxford Diffraction, *CrysAlisPro Software System*, Rigaku Corporation.
19 G. M. Sheldrick, *Acta Crystallogr., Sect. C: Struct. Chem.*, 2015, **71**, 3–8.
20 O. V. Dolomanov, L. J. Bourhis, R. J. Gildea, J. A. K. Howard and H. Puschmann, *J. Appl. Crystallogr.*, 2009, **42**, 2583–2593.
21 K. Brandenburg, *DIAMOND*, Crystal Impact GbR.
22 A. L. Spek, *J. Appl. Crystallogr.*, 2003, **36**, 7–13.
23 B. L. Schottel, J. Bacsa and K. R. Dunbar, *Chem. Commun.*, 2005, 46–47.
24 S. Demeshko, S. Dechert and F. Meyer, *J. Am. Chem. Soc.*, 2004, **126**, 4508–4509.
25 D. D. Hadži and S. Bratos, The Hydrogen Bonds, Recent Developments in Theory and Experiments, in *Vibrational Spectroscopy of the Hydrogen Bond*, 1976, vol. 2.
26 G. Bator and L. Sobczyk, *Wiad. Chem.*, 2011, **65**, 869–885.
27 L. L. Samorjai and D. Hornig, *J. Chem. Phys.*, 1980, **1962**, 36.
28 S. Kumar, A. K. Rai, S. Rai, D. Rai, A. Singh and V. Singh, *J. Mol. Struct.*, 2006, **791**, 23–29.
29 M. Kątcka and T. Urbański, *Bull. Acad. Pol. Sci., Ser. Sci. Chim.*, 1964, **XII**, 615.
30 M. Wojtaś, G. Bator and J. Baran, *Vib. Spectrosc.*, 2003, **15**, 5765–5781.
31 Y. Lien and W. Nawar, *J. Food Sci.*, 1974, **79**, 911–913.
32 A. Schaberg, R. Wroblowski and R. Goertz, *J. Phys.: Conf. Ser.*, 2018, **1107**, 032013–032018.
33 S. Kalinin, A. Rar and S. Jesse, *IEEE Trans. Ultrason. Ferroelectr. Freq. Control*, 2008, **53**, 2226–2252.
34 E. Eliseev, S. Kalinin, S. Jesse, S. Bravina and A. Morozovskaa, *J. Appl. Phys.*, 2007, **102**, 014109.
35 I. Bdikin, J. Gracio, R. Ayouchi, R. Schwarz and A. L. Kholkin, *Nanotechnology*, 2010, **21**, 235703.

36 J. F. Nye, *Physical Properties of Crystals*, Clarendon Press, 1957.
37 S. J. Grabowski, *J. Phys. Org. Chem.*, 2004, **17**, 18–31.
38 R. Surekha, R. Gunaseelan, P. Sagayaraj and K. Ambujam, *CrystEngComm*, 2014, **16**, 7979.
39 W. Bi and N. Mercier, *Chem. Commun.*, 2008, 5743–5745.
40 R. A. Ganeev, *Nonlinear Optical Properties of Materials*, Springer, Berlin, Heidelberg, New York, 2000.
41 A. S. Tayi, A. Kaeser, M. Matsumoto, T. Aida and S. I. Stupp, *Nat. Chem.*, 2015, **7**, 281.
42 Directive 2002/95/EC of the European Parliament and of the Council, Official Journal of the European Union.